COMPARATIVE STUDY OF MICROSTRUCTURAL AND MECHANICAL PROPERTIES OF TWO DIRECTIONALLY SOLIDIFIED INTERMETALLIC NICKEL-BASED ALLOYS

JURAJ LAPIN[1]

Microstructure, hardness, room-temperature tensile properties, high-temperature compressive properties, and creep of two directionally solidified and annealed multiphase intermetallic alloys with chemical composition Ni-21.7Al-7.5Cr-6.5Ti and Ni-20.2Al-8.2Cr-2.4Fe [at.%] were studied. The microstructure of both as-grown alloys consisted of $\gamma'(Ni_3Al)$-phase, γ-phase (Ni-based solid solution), β(NiAl)-phase and α-Cr precipitates. Microstructural changes observed during annealing significantly increased room-temperature yield stress of the alloy with addition of Ti and ductility of the alloy with addition of Fe. The compressive yield stress increased with increasing temperature, reaching peak values at about 700 and 760 °C for the alloy modified by Ti and Fe, respectively. For both alloys the creep stress exponent was determined to vary between 4.0 and 4.5 over the studied temperature range from 700 to 877 °C. The apparent activation energy for creep was calculated to be 380 and 316 $kJ \cdot mol^{-1}$ for the alloy modified by Ti and Fe, respectively.

K e y w o r d s: multiphase intermetallics, mechanical properties, phase transformations, microscopy

POROVNÁVACIA ŠTÚDIA MIKROŠTRUKTÚRNYCH A MECHANICKÝCH VLASTNOSTÍ DVOCH USMERNENE KRYŠTALIZOVANÝCH INTERMETALICKÝCH ZLIATIN NA BÁZE NIKLU

Študovali sme mikroštruktúru, tvrdosť, mechanické vlastnosti v ťahu pri izbovej teplote, vlastnosti v tlaku pri vyšších teplotách a creep dvoch usmernene kryštalizovaných a žíhaných polyfázových intermetalických zliatin s chemickým zložením Ni-21,7Al-7,5Cr-6,5Ti a Ni-20,2Al-8,2Cr-2,4Fe [at.%]. Mikroštruktúra obidvoch zliatin po usmernenej kryštalizácii pozostávala z intermetalickej fázy $\gamma'(Ni_3Al)$, tuhého roztoku na báze niklu γ, intermetalickej fázy β(NiAl) a precipitátov α-Cr. Mikroštruktúrne zmeny v priebehu

[1]Institute of Materials and Machine Mechanics, Slovak Academy of Sciences, Račianska 75, 831 02 Bratislava 3, Slovak Republic, e-mail: ummslapi@savba.sk

žíhania významne zvýšili medzu sklzu zliatiny legovanej Ti a ťažnosť pri izbovej teplote zliatiny legovanej Fe. Medza sklzu v tlaku sa zvyšovala so zvyšujúcou sa teplotou, maximálnu hodnotu dosiahla pri teplote 700 °C pri zliatine legovanej Ti a pri teplote 760 °C pri zliatine legovanej Fe. V študovanom intervale creepových teplôt od 700 do 877 °C sa napäťový exponent pre obidve zliatiny menil v intervale od 4 po 4,5. Vypočítali sme zdanlivú aktivačnú energiu creepu 380 $kJ \cdot mol^{-1}$ pre zliatinu legovanú Ti a 316 $kJ \cdot mol^{-1}$ pre zliatinu legovanú Fe.

1. Introduction

Multiphase intermetallic alloys based on the Ni-Al-Cr system are potential materials for high-temperature structural applications. These alloys can provide a good combination of room-temperature ductility, oxidation resistance, strength and creep resistance that cannot be achieved in monolithic intermetallics [1–8]. In spite of previous studies, very little work has been carried out on directionally solidified (DS) multiphase alloys and studies of microstructure and mechanical properties of these materials are still lacking in the literature. Directional solidification represents another successful approach not only to achieve ductility in even Al-rich Ni_3Al but to produce complex near net shape parts as well. Therefore, investigations of microstructure and mechanical behaviour of DS multiphase nickel-based alloys are of great interest.

The aim of the present paper is to study microstructural and mechanical properties of two DS nickel-based intermetallic alloys modified with additions of chromium, titanium and iron. Chromium and iron are known to partition equally between Ni and Al sites and titanium in Al site in Ni_3Al. On the other hand, chromium tends to disorder Ni_3Al and stabilise the disordered γ-phase in the microstructure. The selected alloys represent two developing groups of multiphase nickel aluminides with significantly different room-temperature ductility after directional solidification and heat treatments.

2. Experimental procedure

The master ingots of intermetallic alloys with chemical compositions Ni-21.7Al-7.5Cr-6.5Ti (Alloy A) and Ni-20.2Al-8.2Cr-2.4Fe (Alloy B) [at.%] were prepared by exo-melt process and cast into graphite moulds in an induction furnace with an argon atmosphere. After casting the ingots were machined to rods with a length of 120 mm and placed into high purity alumina crucibles of 11/15 mm (inside/outside) diameters. Directional solidification was performed under an argon atmosphere in a modified Bridgman-type apparatus [9]. Specimens were directionally solidified at constant growth rates V varying in the range from 2.78×10^{-6} to 1.18×10^{-4} $m \cdot s^{-1}$ and a constant temperature gradient in the liquid at the solid-liquid interface of $G_L = 15 \times 10^3$ $K \cdot m^{-1}$.

Tensile specimens with a gauge length of 16 mm and gauge diameter of 4 mm were lath-machined from the as-grown and annealed ingots. The tensile axis

of specimens was parallel to the growth direction of dendrites or lamellae. The tensile tests were performed on the specimens annealed in the temperature range from 700 to 1200 ℃ for 100 h in air. Before tensile tests the Vickers hardness measurements were performed at load of 98.1 N. Tensile room temperature tests were conducted on a screw-driven Zwick machine at an initial strain rate of 1.04×10^{-3} s^{-1}. The offset yield stress was measured at 0.2 % plastic strain and the ductility was evaluated from the total elongation to fracture.

Compression specimens with a diameter of 8 mm and length of 12 mm were machined with the compression axis parallel to dendrite or lamellae growth direction. Compression tests were performed with a computer-controlled universal testing machine at strain rates of 2.78×10^{-3} and 2.78×10^{-4} s^{-1}. The tests were run at temperatures ranging from 500 to 1000 ℃ in air. The offset yield stress was measured at 0.2 % plastic strain.

Creep specimens with a gauge length of 20 mm and gauge diameter of 4 mm were machined from the as-grown ingots. Before creep tests the creep specimens of Alloy A and Alloy B were annealed at 1000 and 900 ℃ for 100 h in air, respectively. Constant load creep tests were performed at the temperatures ranging from 700 to 877 ℃ under tensile stresses ranging from 100 to 350 MPa in air. Specimen displacement was measured using a linear variable displacement transformer (LVDT) that was attached to the ridges of the creep specimens.

Microstructural analysis was performed by scanning electron microscopy (SEM), energy dispersive spectroscopy (EDS) and transmission electron microscopy (TEM). Samples for TEM were thinned mechanically to a thickness of 100 μm and then by ion milling using dual guns operated at 5 kV with a current of 500 μA per gun. TEM investigations were conducted using JEM-100C microscope equipped with an energy dispersive X-ray spectrometer KEVEX.

3. Results and discussion

3.1 Microstructure of the as-grown and annealed alloys

After directional solidification at constant growth rates ranging from $2.78 \times \times 10^{-6}$ to 1.18×10^{-4} $m \cdot s^{-1}$ the structure of Alloy A contained several columnar grains (3–4) elongated in a direction parallel to the ingot axis. The microstructure within the grains consisted of dendrites with well developed secondary dendrite arms and interdendritic region, as seen in Fig. 1. The primary dendrite arm spacing λ_1 decreased proportionally with the growth rate according to relationship $\lambda_1 \propto \propto V^a$, where the value of the rate exponent a was calculated to be -0.23 ± 0.04. The average volume fraction of dendrites was measured to be about 50 vol.%. Fig. 2 shows typical microstructure of the alloy. TEM and EDS observations revealed that the dendrites are composed of β(B2)-matrix (NiAl), coarse $\gamma'(L1_2)$-particles (Ni_3Al), fine γ'-needles, and spherical α(A2)-precipitates (Cr-based solid solution).

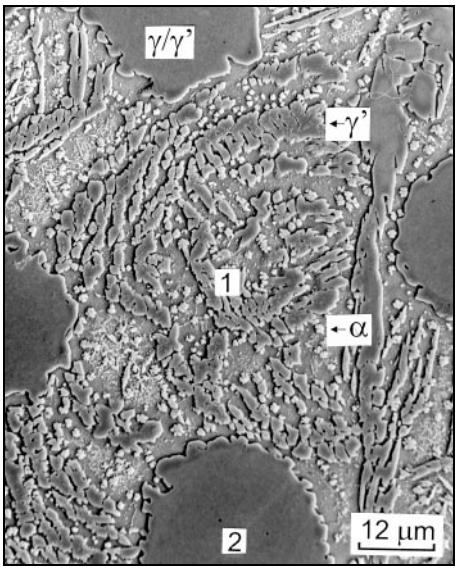

Fig. 1. SEM micrograph showing dendritic morphology of DS Alloy A: $V = 2.78 \times 10^{-5}$ m·s^{-1}, 1 – dendrite, 2 – interdendritic region.

Fig. 2. Backscattered SEM micrograph showing coexisting phases in DS Alloy A, $V = 2.78 \times 10^{-5}$ m·s^{-1}.

The interdendritic region contained ordered domains of γ'-phase surrounded by γ(A1)-matrix (Ni-based solid solution) and lath-shaped α-precipitates. The lath-shaped α-precipitates nucleated only from the disordered γ-phase. The annealing in the temperature range from 700 to 1200 ℃ significantly affected the microstructure of DS alloy. The as-grown dendritic structure was unstable and initial volume fraction of dendrites decreased during annealing from about 50 vol.% measured in the as-grown material to a minimum value of about 38 vol.% after ageing at 1100 ℃ for 300 h. Annealing at a higher temperature of 1200 ℃ resulted in stabilisation of the β-phase, and stable dendrite volume fraction was reached after 50 h ageing. Annealing at temperatures of 1100 and 1200 ℃ resulted in unusual coarsening of the α-precipitates and formation of α "flowers", as shown in Fig. 3.

On the contrary, the microstructure of Alloy B directionally solidified at a growth rate of 4.17×10^{-6} m·s^{-1} consisted of multiple columnar eutectic grains. Fig. 4 shows typical microstructure of this alloy. Within each grain, well aligned and equally spaced lamellae with an average thickness of 2.4 μm and volume fraction of 16 vol.% were observed. A small amount of fibres with average diameter of 2 μm was distributed along some grain boundaries. Higher growth rate of 5.56×10^{-6} m·s^{-1} resulted in breakdown of aligned eutectic growth and formation

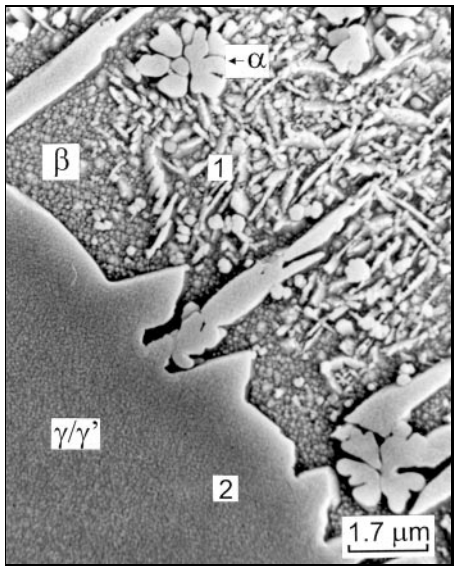

Fig. 3. SEM micrograph showing α "flowers" after annealing at 1100 °C for 200 h: $V = 2.78 \times 10^{-5}$ m·s^{-1}, 1 – dendrite, 2 – interdendritic region.

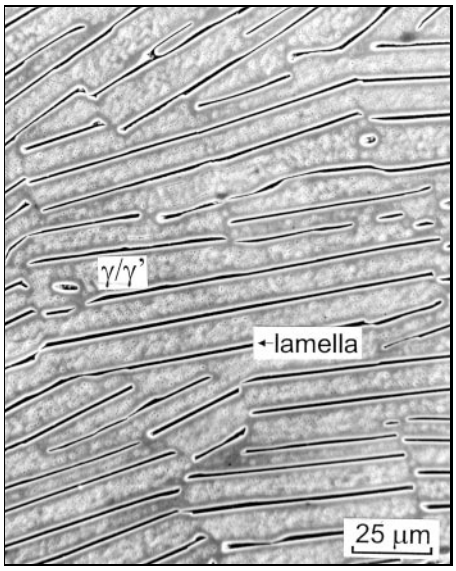

Fig. 4. SEM micrograph of the transverse section of Alloy B directionally solidified at $V = 4.17 \times 10^{-6}$ m·s^{-1} showing lamellar eutectic grains.

of irregular lamellae and fibres. The lamellae were composed of β-phase, some $L1_0$ type martensite (β'-phase) and spherical α-Cr precipitates, as seen in Fig. 5 [10]. The interlamellar region consisted of single γ'-layer formed around lamellae and three-phase region composed of γ'-precipitates, γ-phase and fine lath-shaped α-Cr precipitates. Annealing at 750 °C resulted in an intensive transformation of γ-phase to γ'-phase and further precipitation of fine lath-shaped α-Cr particles in the interlamellar region. Annealing at 850 °C significantly decreased the volume fraction of lamellae, which was connected with an intensive precipitation of lath-shaped α-Cr particles with average length of $l = 2$ μm and width of $h = 0.1$ μm in the interlamellar regions, as shown in Fig. 6. These precipitates were significantly coarser ($l = 3$ μm and $h = 0.2$ μm) after annealing at 900 °C. In this case, majority of lamellae transformed to the continuous γ'-layer and volume fraction of γ-phase was significantly reduced to about 4 vol.%. Annealing at 950 °C stabilised lamellae with coarse spherical α-Cr precipitates. The interlamellar regions contained elongated areas of γ-phase (9 vol.%). The volume fraction of single γ'-layer around the lamellae increased at the expense of decreasing volume fraction of the interlamellar regions. Annealing at 1050 °C stabilised the lamellae and significantly reduced the amount of α-Cr precipitates in the microstructure. Annealing at 1100 °C resulted

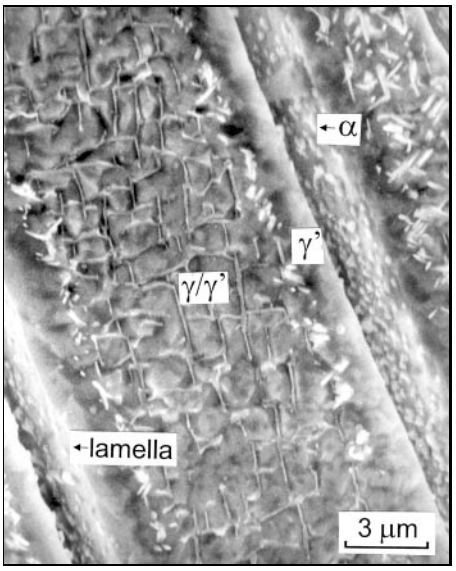

Fig. 5. SEM micrograph showing typical microstructure of Alloy B, $V = 4.17 \times 10^{-6}$ m·s^{-1}.

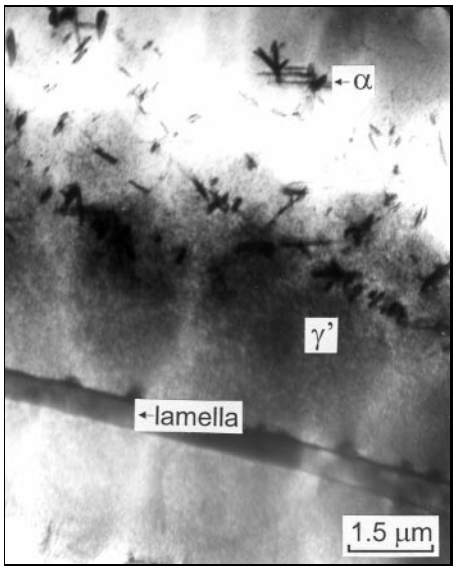

Fig. 6. TEM micrograph of lamellae and the lath-shaped α-Cr precipitates formed in the γ/γ'-interlamellar region, $V = 4.17 \times 10^{-6}$ m·s^{-1}.

in formation of new γ/γ'-regions in the vicinity of the lamellae.

Detailed crystallographic study of orientation relationships between coexisting phases in the studied alloys in the as-grown and annealed state was performed by Lapin et al. [10, 11]. In spite of the fact that the studied alloys were prepared at relatively slow cooling rates, the same orientation relationships were determined by Iždinský et al. [12, 13] in plasma sprayed and annealed Ni-Al-Cr based coatings.

3.2 Effect of annealing on the hardness

Fig. 7 shows the results of Vickers' hardness measurements performed on the samples annealed at various temperatures for 100 h. For the as-grown alloys, significantly higher hardness of Alloy A can be attributed to higher volume fraction of harder β-phase (50 vol.% of dendrites containing β-phase) in comparison with that in Alloy B (16 vol.% of lamellae containing β-phase) and to an intensive solid solution hardening of the γ'-phase by Ti. Extensive precipitation of fine α- and γ'-particles resulted in significant increase of hardness during annealing at 700 °C of Alloy A and at 750 °C of Alloy B. As shown by Tian et al. [14], precipitation of fine coherent spherical α-particles significantly increases hardness of β-phase.

In addition, transformation of the γ to γ' and precipitation hardening of the γ'-matrix by fine lath-shaped α-particles significantly increased the hardness of the γ/γ'-regions. As was revealed by TEM observations, these transformations were connected with a significant increase of the dislocation density within the γ'-phase [11]. The loss of coherency of the α-precipitates, coarsening of the α-particles and decreasing volume fraction of the β-phase resulted in softening of both materials connected with a decrease of hardness. For both alloys, a minimum hardness was achieved after annealing at about 950 °C.

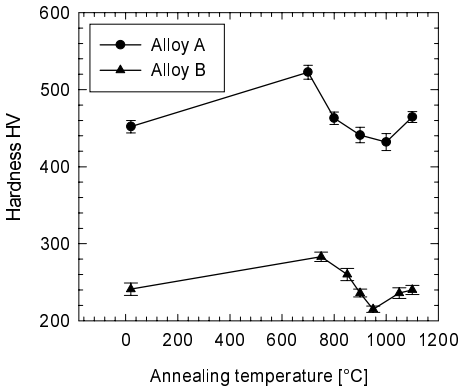

Fig. 7. Variation of the hardness with annealing temperature for the specimens annealed for 100 h.

Annealing at 1100 °C did not affect significantly hardness of the alloys in comparison with the as-grown state. It should be noted that at this temperature the β-phase with spherical α-particles was stabilised in the microstructure of both alloys.

3.3 Room-temperature tensile properties

Fig. 8 shows the dependence of the offset yield stress and ultimate tensile stress (UTS) on the annealing temperature for Alloy A directionally solidified at $V = 2.78 \times 10^{-5}$ m·s^{-1} and Alloy B directionally solidified at $V = 4.17 \times 10^{-6}$ m·s^{-1} after annealing for 100 h. Fig. 9 shows the variation of room-temperature tensile elongation with the annealing temperature. It should be noted that the data shown in Figs. 8 and 9 represent average values from four tensile specimens tested for each alloy and annealing temperature.

For Alloy A, annealing at 700 °C significantly decreased tensile ductility in comparison with the as-grown alloy, which resulted in a premature fracture of tensile specimens without measurable 0.2 % offset yield stress. A maximum of the yield stress and UTS was achieved after annealing at 800 °C. The highest tensile ductility (about 1 %) was achieved in the as-grown alloy and all structural changes observed in the annealed material lowered the ductility.

For Alloy B, annealing at 800 °C slightly increased the yield stress and decreased the total elongation to fracture but had no influence on the ultimate tensile stress in comparison with the as-grown specimens. A significant decrease of the yield stress and increase of the elongation was observed after annealing at 900 and 950 °C. Annealing at 1050 and 1100 °C had no influence on the yield stress, decreased the ultimate tensile stress and increased the ductility in comparison with

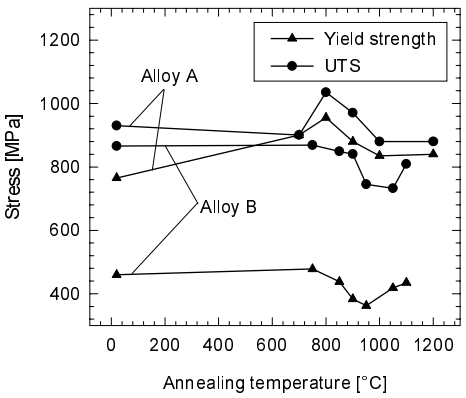

Fig. 8. Dependence of the offset yield stress and ultimate tensile stress (UTS) on the annealing temperature for tensile specimens annealed for 100 h.

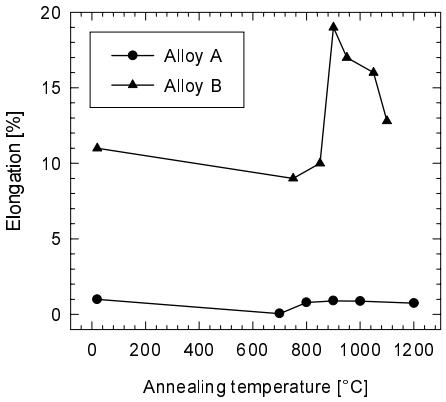

Fig. 9. Dependence of the room-temperature tensile elongation on the annealing temperature for tensile specimens annealed for 100 h.

the as-grown specimens.

A significantly lower tensile ductility of Alloy A in comparison with Alloy B can be explained by the slip transfer from more ductile γ/γ'-interdendritic region with higher elastic modulus and lower yield stress to the β-phase [8, 11]. During uniform straining of both components, the stresses carried by the γ'-matrix are higher than those of dendrites. The dislocations generated in the γ'-matrix on the $\{111\}$ slip planes start piling up at the dendritic-interdendritic (Alloy A) or interlamellar--lamellar (Alloy B) interfaces. Pile-up stresses in the γ'-matrix can preferentially nucleate dislocations on softer $\{110\}\langle 001\rangle$ instead of harder $\{110\}\langle 111\rangle$ slip systems of the β-phase. However, such slip transfer was not achieved in Alloy A due to obstacles to dislocation motion in the β-phase. Alloying by chromium and titanium resulted in a significant solution and precipitation strengthening of the β-phase. Therefore, critical resolved shear stress for possible slip systems was higher than cleavage stress of the β-phase. Therefore, instead of slip transfer, cracks nucleation and their growth occurred in the β-phase, as seen in Fig. 10. On the contrary, the slip transfer from γ/γ'-matrix to the β-phase was effective in the case of Alloy B resulting in high room-temperature elongation (up to 19 %). Fig. 11 shows that the interlamellar-lamellar interfaces served as crack nucleation sites also for Alloy B. However, the nucleation and growth of cracks occurred at significantly higher tensile elongation in comparison with that of Alloy A.

3.4 High-temperature compressive properties

Fig. 12 shows the evolution of the offset yield stress as a function of tempera-

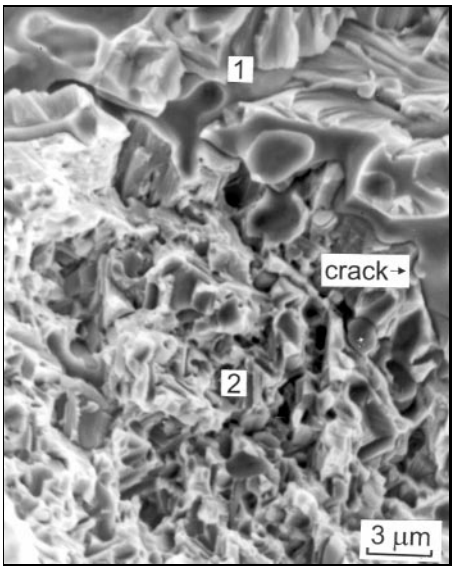

Fig. 10. SEM micrograph showing typical features of fracture surface of Alloy A, $V = 5.56 \times 10^{-5}$ m·s^{-1}, 1 – dendrite, 2 – interdendritic region.

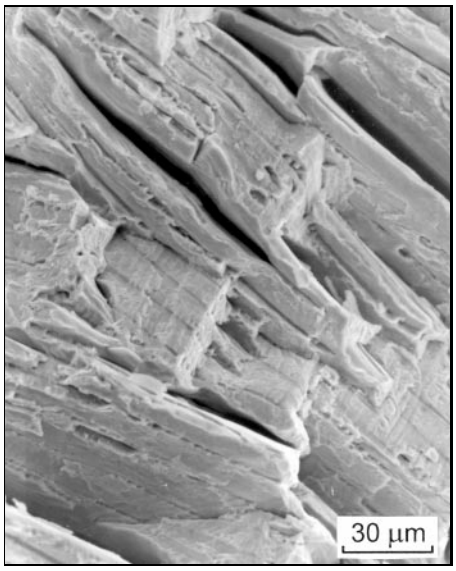

Fig. 11. SEM micrograph showing typical features of fracture surface of Alloy B, $V = 4.17 \times 10^{-6}$ m·s^{-1}.

ture and strain rate. As seen in this figure, addition of 6.5 at.% of titanium significantly increased the yield stress of Alloy A in comparison with Alloy B. For both alloys the compressive yield stress initially increased with the temperature reaching a peak value at about 700 and 760 °C for Alloy A and Alloy B, respectively. This indicates that the yield stress was dominated by the γ'-phase. Similar compressive behaviour was observed in β/γ'-alloy by Misra et al. [8]. A rapid decrease of the yield stress in Alloy B at higher temperatures was connected with transformation of lamellae, precipitation of α-Cr particles and morphological changes of the γ- and γ'-phases [10].

Fig. 13 shows the temperature evolution of the yield stress for several Ni_3Al alloys modified by Cr, Ti and Nb (solid solution hardening elements) [15]. All alloys show an anomalous yielding behaviour characterised by increasing yield stress with increasing temperature reaching peak values at a critical temperature T_c. The critical temperature depends on the alloying elements. In spite of the fact that multiphase Alloy A shows lower T_c than single phase alloy modified by Ti and Cr a decrease of the yield stress at temperatures higher than T_c is more smooth. This high-temperature strength is achieved by stabilisation of a relatively high volume fraction of precipitation strengthened β-phase in the microstructure.

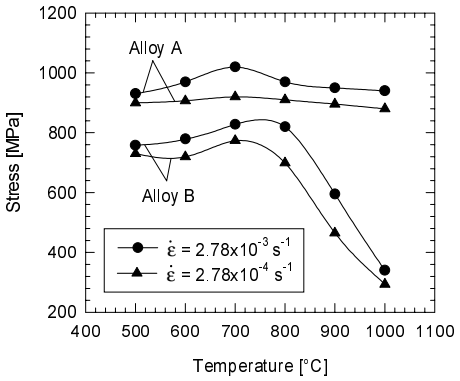

Fig. 12. Temperature dependence of compressive yield stress.

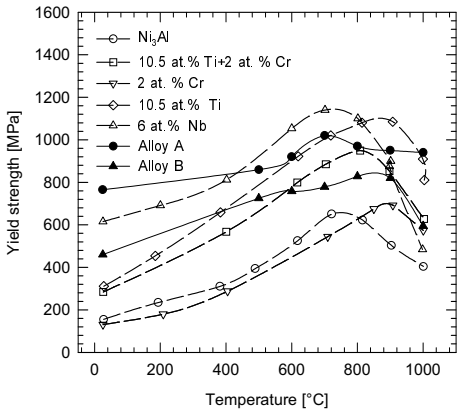

Fig. 13. Temperature dependence of the yield stress of several Ni_3Al alloys according to Ref. [15] and the studied Alloy A and Alloy B.

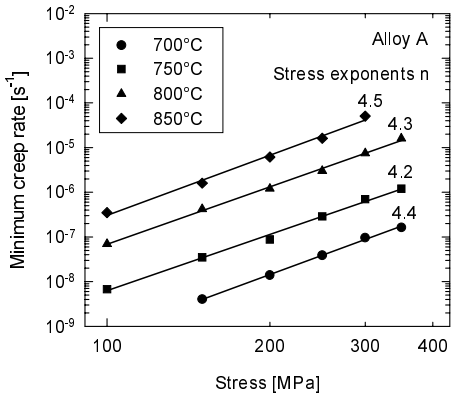

Fig. 14. Minimum creep rate as a function of applied stress for Alloy A.

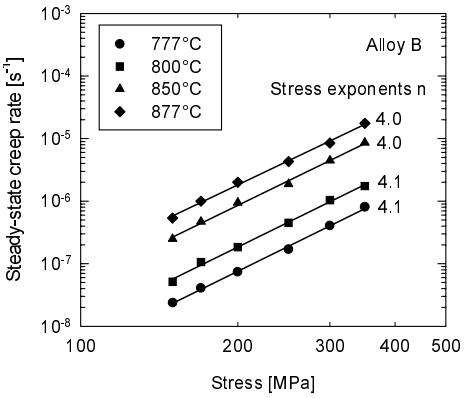

Fig. 15. Steady-state creep rate as a function of applied stress for Alloy B.

3.5 Creep properties

The creep curves of both alloys exhibited a short inverse primary creep stage that was followed by tertiary creep stage (Alloy A) or by steady-state creep (Alloy B). Measured minimum creep rates $\dot{\varepsilon}_{\min}$ and steady-state creep rates $\dot{\varepsilon}_{\mathrm{s}}$ were fitted to the power law in a general form

$$\dot{\varepsilon}_{\mathrm{a}} = A\sigma^n, \tag{1}$$

where σ is the applied stress, n is the stress exponent and subscript a corresponds to min in the case of Alloy A and to s in the case of Alloy B. Fig. 14 shows the dependence of minimum creep rate on the applied stress for Alloy A. Fig. 15 illustrates the dependence of steady-state creep rate on the applied stress for Alloy B. The stress-creep rate-temperature data were also fitted to the Bailey-Norton power law expression

$$\dot{\varepsilon}_{\mathrm{a}} = B\sigma^n \exp(-Q_{\mathrm{a}}/RT), \tag{2}$$

where B is a constant, Q_{a} is the apparent activation energy for creep, R is the universal gas constant and T is the absolute temperature. The apparent activation energy for creep Q_{a} calculated for the six different stresses at four different temperatures was 380 ± 10 and 316 ± 9 kJ·mol^{-1} for Alloy A and Alloy B, respectively. The calculated stress exponents and activation energies for creep are comparable with those measured by other authors [16–20] for Ni_3Al-based alloys where n was determined to vary from 2.6 to 4.4 and Q_{a} varied from 316 to 540 kJ·mol^{-1}, as recently summarised by Lapin [7]. It should be noted that the activation energy for creep of Alloy A is higher than the activation energy for lattice diffusion Q_{L} of Ni in Ni_3Al reported by Frank et al. [21] for a binary system ($Q_{\mathrm{L}} = 303$ kJ·mol^{-1}) or Bokstein et al. [22] for an alloyed Ni_3Al ($Q_{\mathrm{L}} = 305$ kJ·mol^{-1}).

Fig. 16 summarises graphically the dependence of creep rate normalised by the apparent activation energy for creep and temperature as a function of the applied stress. Linear regression analysis of the creep data yields the creep equation in the form

$$\dot{\varepsilon}_{\mathrm{min}} = 508.57\sigma^{4.3} \exp(-380000/RT) \tag{3}$$

for Alloy A and in the form

$$\dot{\varepsilon}_{\mathrm{s}} = 0.192\sigma^{4.1} \exp(-316000/RT) \tag{4}$$

for Alloy B. The regression coefficients of these fits r^2 are better than 0.98. As results from Eqs. (3) and (4), Alloy A exhibits minimum creep rates about one order of magnitude higher than the steady-state creep rates measured in Alloy B at the same creep conditions.

It should be noted that the creep of the studied alloys can be analysed in terms of temperature dependence of elastic modulus and assuming interactions of reinforcing particles with the dislocations (threshold stress) as reported by Čadek et al. [23–25] and Rösler and Arzt [26, 27] for particle strengthened alloys. Such analysis allows to identify true activation energy for creep and controlling mechanisms of creep deformation [7].

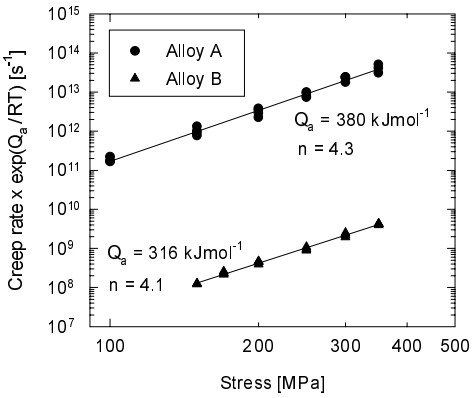

Fig. 16. Comparison of the creep rates normalised by the apparent activation energy for creep and temperature as a function of the applied stress for Alloy A and Alloy B.

4. Conclusions

Two DS Ni-Al-Cr type alloys modified with additions of titanium and iron were compared. The following conclusions were reached:

1. The microstructure of both as-grown alloys consisted of $\gamma'(Ni_3Al)$-phase, γ-phase (Ni-based solid solution), β(NiAl)-phase and α-Cr precipitates. The annealing in the temperature range from 700 to 1200 ℃ significantly affected the as-grown microstructure of DS alloys.

2. Microstructural changes observed during annealing significantly affected hardness and room-temperature tensile properties of the alloys. The alloy modified by Ti showed significantly higher yield stress and lower tensile ductility than the alloy modified by Fe.

3. The compressive yield stress increased with increasing temperature, reaching peak values at about 700 and 760 ℃ for the alloy modified by Ti and Fe, respectively, and decreased at higher temperatures.

4. The creep rate was found to depend on the applied stress and temperature. For both alloys the power law stress exponent was determined to vary between 4.0 and 4.5 over the studied temperature range. The apparent activation energy for creep was calculated to be 380 and 316 kJ/mol for the alloy modified by Ti and Fe, respectively.

Acknowledgements

The author gratefully acknowledges the financial support of the Slovak Grant Agency for Science under the VEGA contract 2/1044/21.

REFERENCES

[1] CAHN, R. W.: Phil. Trans. R. Soc. Lond., *A351*, 1995, p. 497.
[2] YANG, R.—LEAKE, J. A.—CAHN, R. W.: Phil. Mag., *A65*, 1992, p. 961.

[3] YANG, R.—LEAKE, J. A.—CAHN, R. W.: Mater. Sci. Eng. A, *A152,* 1992, p. 227.
[4] SIKKA, V. K.—DEEVI, S. C.—VISWANATHAN, S.—SWINDEMAN, R. W.—SANTELLA, M. L.: Intermetallics, *8,* 2000, p. 1329.
[5] PÉREZ, P.—GONZÁLEZ, P.—GARCÉS, G.—CARUANA, G.—ADEVA, P.: J. Alloy Compd., *302,* 2000, p. 137.
[6] LAPIN, J.: Intermetallics, *5,* 1997, p. 615.
[7] LAPIN, J.: Intermetallics, *7,* 1999, p. 599.
[8] MISRA, A.—GIBALA, R.—NOEBE, R. D.: Metall. Mater. Trans. A, *A30,* 1999, p. 1003.
[9] LAPIN, J.: Kovove Mater., *34,* 1996, p. 265.
[10] LAPIN, J.—WIERZBINSKI, S.—PELACHOVÁ, T.: Intermetallics, *7,* 1999, p. 705.
[11] LAPIN, J.—PELACHOVÁ, T.—BAJANA, O.: Intermetallics, *8,* 2000, p. 1417.
[12] IŽDINSKÝ, K.—IVAN, J.—ZEMÁNKOVÁ, M.: Kovove Mater., *38,* 2000, p. 329.
[13] IŽDINSKÝ, K.—IVAN, J.—ZEMÁNKOVÁ, M.: Kovove Mater., *39,* 2001, p. 316.
[14] TIAN , W. H.—HAN, C. S.—NEMOTO, M.: Intermetallics, *7,* 1999, p. 59.
[15] THORNTON, P. H.—DAVIES, R. G.—JOHNSTON, T. L.: Metall. Trans., *1,* 1970, p. 207.
[16] FLINN, P. A.: Trans. TSM-AIME, *218,* 1960, p. 145.
[17] NICHOLLS, J. R.—RAWLINGS, R. D.: J. Mater. Sci., *12,* 1977, p. 2456.
[18] NATHAL, M. V.—DIAZ, J. O.—MINER, R. V.: Mater. Res. Soc. Symp. Proc., *133,* 1989, p. 269.
[19] WOLFENSTINE, J.—KIM, H. K.—EARTHMAN, J. C. : Scripta Metall. Mater., *26,* 1992, p. 1823.
[20] WOLFENSTINE, J.—KIM, H. K.—EARTHMAN, J. C.: Metall. Mater. Trans. A, *25A,* 1994, p. 2477.
[21] FRANK, S.—RÜSING, J.—HERZIG, C.: Intermetallics, *4,* 1996, p. 601.
[22] BOKSTEIN, B. S.—BOKSTEIN, S. Z.—SPITSBERG, I. T.: Intermetallics, *4,* 1996, p. 517.
[23] ČADEK, J.—KUCHAŘOVÁ, K.—ZHU, S.: Kovove Mater., *39,* 2001, p. 77.
[24] ČADEK, J.—KUCHAŘOVÁ, K.—ZHU, S.: Kovove Mater., *39,* 2001, p. 221.
[25] ČADEK, J.—KUCHAŘOVÁ, K.—ZHU, S.: Kovove Mater., *38,* 2000, p. 130.
[26] RÖSLER, J.—ARZT, E.: Acta Metall., *36,* 1988, p. 1043.
[27] RÖSLER, J.—ARZT, E.: Acta Metall., *38,* 1990, p. 671.

Received: 21.1.2002